Arch. Metall. Mater. **63** (2018), 1, 347-357

DOI: 10.24425/118947

J. WANG*, Y. ZHANG*#, B. SHI*, Q. ZHAO*, Q. SUN*, Z. ZHANG*, H. LU*,**

FATIGUE BEHAVIOR AND MECHANISM OF FV520B-I OWING TO THE EFFECT OF LOADING FREQUENCY ON THE FATIGUE PROPERTY IN HCF AND VHCF REGIME

Fatigue property of FV520B-I is affected by the ultrahigh loading frequency significantly, and the ultrasonic fatigue experimental data can't be employed directly to analyze the fatigue failure in the actual remanufacturing engineering. However few theories about the effect of loading frequency on the fatigue property of FV520B-I has ever been proposed. In this paper, both ultrasonic experiment and conventional experiment are conducted out to obtain the fatigue data. The effect of loading frequency on the fatigue data distribution is discussed firstly, its fatigue limit declines with the increase of the loading frequency. Then the fracture surface observations are captured, the fatigue property and fatigue behavior mechanism of FV520B-I is examined by analyzing the fracture surface features, crack initiation and failure observations. A new material frequency correction factor is proposed and introduced to eliminate the influence of the loading frequency on the FV520B-I fatigue property. FV520B-I empirical fatigue life conversion model and fatigue strength conversion model are established with comprehensive use of a fitting algorithm based on the combination of experimental data and classic formula. A clear understand of the effect of loading frequency on the fatigue property of FV520B-I is novel and has an important significance in guaranteeing the accuracy of the actual fatigue analysis of FV520B-I in the remanufacturing engineering.

Keywords: ultrahigh loading frequency; FV520B-I; fatigue strength; fatigue conversion model

1. Introduction

High strength metal FV520B-I has numerous positive mechanical properties including high strength, high corrosion resistance, high abrasive resistance and good welding characteristics [1]. As a result, FV520B-I is widely adopted in the manufacturing of centrifugal compressor vanes. The manufactured vanes are generally used under cyclic loading conditions. So, the fatigue life of the used FV520B-I is often over 10^7 cycles, and even reaches 10^9 or 10^{10} cycles, a "very high cycle-cycle" fatigue level [2-4]. In normal working conditions, the high cycle-fatigue failure happens instantaneously without any warnings and it is also irreversible. Fatigue failure can easily cause serious accidents [5-7], which lead to tremendous economic loss, significant impact on the mechanical system, and can even threaten human life. A clear understanding of the fatigue property of FV520B-I in engineering practice is essential in remanufacturing engineering process of FV520B-I.

The objective of this fatigue experimental study is to better understanding the mechanism of FV520B-I fatigue properties. The experimental loading frequency is the main concern of the restriction of the further development in fatigue experiments [8-9]. For example, it takes at least 120 days (4 months) to complete a 10^9 cycles fatigue experiment with 100 Hz, which is inefficient and infeasible. Increasing the experimental loading frequency is the most effective and simplest way to improve the experimental efficiency. With the use of the ultrasonic fatigue experiment system, the experimental loading frequency can be increased from 100Hz to 20 KHz. The efficiency is increased by 200 times [10-11] as that in a conventional experiment. So, the ultrasonic fatigue experiment system makes it possible to complete very high cycle-fatigue experiments in a reasonably short time period.

However, it has been found that the experimental results are affected by an ultrahigh loading frequency [12-15]. There is a significant difference between the experimental data in ultrahigh frequency and in the conventional frequency. In real working conditions, the loading frequency is about 100 Hz to 200 Hz, so the ultrasonic experimental data cannot be directly used to model the actual fatigue failure as a significant difference exists between the ultrasonic loading frequency and the actual engineering loading frequency, especially in actual fatigue life prediction and fatigue strength analysis. Furthermore, the fatigue life prediction and the fatigue strength analysis are the preconditions for remanufacturing of the components. Therefore, the ultrahigh experimental data should be converted into the low loading frequency condition to make a more precise fatigue property analysis (including fatigue life and fatigue strength) and

* SCHOOL OF MECHANICAL ENGINEERING, DALIAN UNIVERSITY OF TECHNOLOGY, DALIAN 116023, P. R CHINA
** COLLEGE OF ENGINEERING, SOUTH DAKOTA STATE UNIVERSITY, BROOKINGS, SD 57007-0001
# Corresponding author: zylgzh@dlut.edu.cn

reasonable remanufacturing in actual engineering. It is necessary to investigate the mechanism of the influence of ultrahigh loading frequency on the experimental data and the fatigue property of FV520B-I in a propose conversion model for FV520B-I.

Quite a few theories have been proposed based on the investigation of the influence of ultrahigh loading frequency on the fatigue property. Ultrasonic fatigue experiment machine has been applied in very high cycle-fatigue experiments on different materials. Wang [16-17] focused on the influence of the loading frequency on the fatigue property of 40Cr and the crack growth rate. It was found that the S-N curve obtained from the ultrahigh loading frequency experiment is higher than the one obtained from the conventional fatigue experiment (50 Hz and 80 Hz). This means that the fatigue life obtained from the ultrahigh loading frequency experiment is longer than the life form the conventional experiment in the same stress amplitude. The difference the experimental results from the two experiments due the influence of loading frequency. Shin [18] and Stanzl [19] carried out the fatigue experiments for 304 stainless steel to investigate the effect of the loading frequency on the crack growth rate. The result showed that ultrahigh loading frequency will slow the crack growth rate, and the fatigue life will be extended. Based on combination of the investigation result and the Forman formula, a new formula with consideration of loading frequency was proposed to describe the fatigue crack growth law. Schmid et al. [20] concluded that the frequency effect was small at the load ratio of 0.1 for a martensitic stainless steel. Zhao et al. [21] discussed the influence of material strength level on frequency dependency of VHCF behavior of a bearing steel, and concluded that lower strength steels showed much higher fatigue strength under ultrasonic cycling. Zhu [22] investigated the effect of loading frequency on the behavior of welded joint for Cr-Ni-Mo-V steel and proposed an analysis model.

These theories and models are helpful to the study of the influence of loading frequency on the fatigue property. But the mechanism of the influence of ultrahigh loading frequency on the FV520B-I fatigue property (including fatigue life and fatigue strength) has not been studied comprehensively. Neither the fatigue conversion models for FV520B-I nor the relevant correction coefficients have been proposed, and these are essential for the application and remanufacturing engineering of FV520B-I. Main research in this paper focuses on the analytical model of fatigue behavior of FV520B-I owing to the effect of loading frequency and the establishments of the fatigue conversion models (including fatigue life conversion model and fatigue strength conversion model) for FV520B-I. Both the conventional and very high cycle-fatigue experiments are carried out to obtain the fatigue data and the fracture surface observations. The fatigue life conversion model for FV520B-I is established by experimental data fit and parameter estimation of the classical fatigue model. The basic fatigue strength model of FV520B-I is modified by involving a new material frequency correction factor. Therefore, a NEW comprehensive fatigue strength conversion model for FV520B-I is established with the combined application of the basic model and the new factor. The material frequency correction factor and the modified parameters into the empirical fatigue models. The proposed model is also validated by a comparison between the models with the converted strength and the real experimental data. This model can be also used to mapping FV520B-I ultrasonic experimental data into the practical engineering data under traditional working conditions. Main research contribution in this study is providing an analytic model of the fatigue data conversion from the ultrasonic experimental data into the engineering conditions with low loading frequency. Thus, the accuracy of real fatigue life prediction under engineering conditions can be well guaranteed and the study can be a model guidance for FV520B-I in design and remanufacturing.

2. Ultrasonic and conventional experiments

2.1. The experiment procedure

Both conventional experiment and ultrasonic experiment are carried out. The experiment process follows the ASTM (American Society for Testing Material) standard, so the experimental results are credible. The design of the specimen should be such that failure occurs in the test section (reduced area as shown in Fig. 2). The standard also indicates that the test machines should have a force-monitoring system, such as a transducer mounted in series with the specimen, or mounted on the specimen itself, unless the use of such a system is impractical due to space or other limitations. And continue the tests until the specimen failure criterion is attained or until a predetermined number of cycles has been applied to the specimen. Failure may be defined as complete separation, as a visible crack at a specified magnification, as a crack of certain dimensions, or by some other criterion. Due to the discrete-time acquisition of experiment data, the data points are not continuous over the time, so a proper design of the experiment and data acquisition chassis (DAC) is necessary in the study of the influence of loading frequency.

So experimental systems are shown in Fig. 1. The ultrasonic fatigue experiment is carried out in USF-2000 ultrasonic fatigue test system (Fig. 1. (a)) with an operating frequency of 20 kHz. Ultrasonic fatigue experiment system has three core components: the ultrasonic generator, transducer, and amplitude transformer. Data acquisition device obtains the response from the specimen and sends it to the analysis unit for signal transformation.

And the conventional fatigue experiment is carried out in PLG-100 (Fig. 1 (b)) with an operating frequency of 140 Hz, to test the fatigue property under tensile-compressive cyclic loading. The main working principles are the magnetic resonance and the optimization of LC oscillation circuit, with the advantage of low energy consumption and no abrasion. These two different systems can both provide the dynamic load and static load respectively, without mutual interference. This system has been widely used in the conventional fatigue test, its accuracy and reliability have been recognized.

The experiments are carried out under room temperature (20°C) and the mean stress is set zero, which presented that the

(a) The ultrasonic fatigue test system

(b) The conventional fatigue test system

Fig. 1. The fatigue test systems

stress ratio $r = -1$. The maximum stress amplitude is 700 MPa and the minimum one is 550 MPa, the interval is 25 MPa. The stress amplitude and the corresponding data are recorded after the fatigue failure occurred.

2.2. The specimen

Standard fatigue test specimen is used in the two experiments. The geometrical shapes of the specimen are different for the different experimental loading frequencies. They both are the hourglass type with a minimum diameter of 4 mm. The details of the geometrical shape are shown in Fig. 2 (a) and Fig. 2 (b).

The heat treatment process of the specimen is: solution treatment for 1 to 1.5h, air cooling; intermediate treatment in the range of 750 - 850°C for 3-3.5h, oil cooling; aging treatment in the range of 470±10°C for 4 to 5h, air cooling. The chemical compositions of the FV520B-I specimen and the mechanical property of FV520BI are displayed in Table 1 and Table 2 as below:

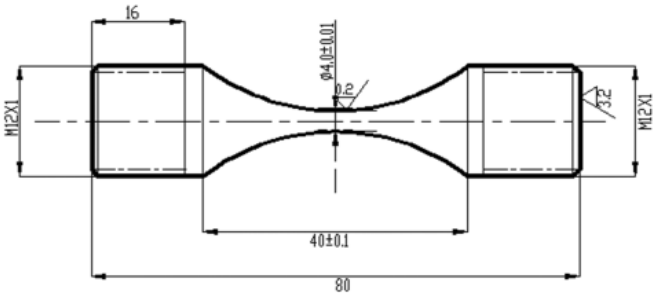

(a) The conventional frequency specimen dimensions

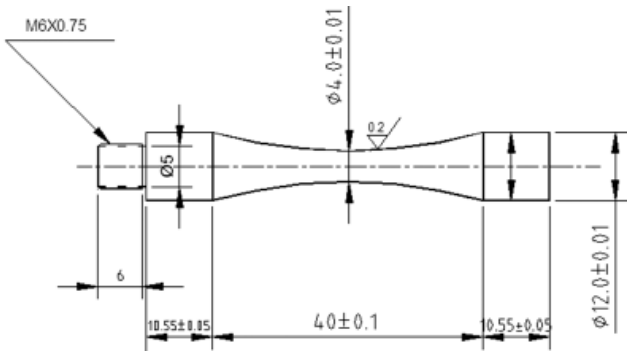

(b) The ultrasonic frequency specimen dimensions

Fig. 2. The specimen used in the experiments

2.3. Experimental results

Fundamental fatigue test data obtained from both conventional experiment and ultrasonic experiment are shown in Fig. 3. Also the *S*-*N* curves at respective loading frequency are depicted.

At 140 Hz, the fatigue experiment will take a long time (several days) to get the very high cycle fatigue because of the low loading frequency. The conventional fatigue experiment was ceased at 7×10^6 cycles. As the experimental difficult, fatigue limit at 140 Hz was evaluated to be 500 MPa. With the consideration of the experimental efficiency, the ultrasonic

TABLE 1

Chemical composition of specimen (wt%)

Chemical composition	Si	C	Ni	Cu	Mn	S	Cr	Mo	Nb	Fe
Specimen	0.15-0.7	0.02-0.07	5-6	1.3-1.8	0.3-1	<0.025	13-14.5	1.3-1.8	0.25-0.45	736.66-76.88

TABLE 2

Mechanical property of FV520B-I

	Elasticity modulus E/GP	Tensile strength Rm/MPa	Yield strength $R_{p0.2}$/MPa	Vickers hardness HV/kgf·mm^{-2}	Elongation A/%	Density ρ/kg·m^{-3}
FV520B-I	194	1180	1029	380	16.07	7.82×10^3

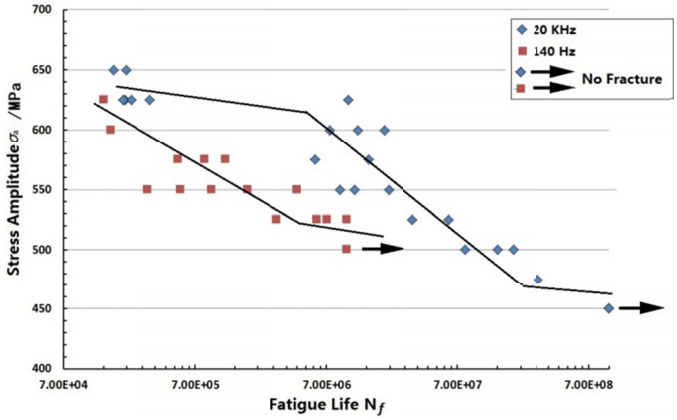

Fig. 3. Experimental data and *S-N* curves

fatigue experiment was ceased at nearly 1×10^8, the fatigue limit at 20 KHz was evaluated to be 450 MPa, smaller than the conventional one. This result is different from existing conclusion [23] that the fatigue limit tends to increase gradually with the increase of the loading frequency and the ultrasonic fatigue limit is bigger than the conventional fatigue limit. It means that the significant increasing of the loading frequency will weaken the fatigue resistance of FV520B-I, but the fatigue life can be extended with the appropriate increase of loading frequency. Another phenomenon showed in Fig. 3 that the experimental data of FV520B-I has an obvious discreteness, small change of the stress amplitude will lead to a significant change of the fatigue life. These two characteristics are due to the special fatigue property of FV520B-I, but few studies have been carried out to investigate the mechanism of this specificity.

Fig. 4 implies the different causes of fatigue failure. Fig. 4. (a) and Fig. 4. (b) are the fracture surface photographs obtained at 140 Hz and 20 KHz respectively under the same stress amplitude. When the stress amplitude is 550 MPa, the conventional fatigue life is 4.21×10^6 cycles and the ultrasonic life is 2.07×10^7, approximately five times bigger than the conventional one.

As shown above, both GBF region and "fish-eye" can be observed clearly in Fig. 4 (b), which implies that the fatigue failure was caused by internal inclusion. However, no such observations can be found from the conventional experimental fracture section, and the primary factor resulted in the surface fatigue failure is the surface defect, especially the surface roughness [24].

When the conventional life and the ultrasonic life are in the same fatigue life magnitudes, the ultrasonic experiment will obtain the bigger stress amplitude than that in conventional experiment. The experimental data also indicate that under the same stress amplitude, the fatigue life obtained from the ultrasonic experiment is longer than the fatigue life obtained from the conventional experiment. As Fig. 5. (a) and Fig. 5. (b) indicate that the fatigue life obtained from these two experiments are about 7×10^6 cycles, the corresponding stress amplitude values are different, 525 MPa for 140 Hz, 600 MPa for 20 KHz.

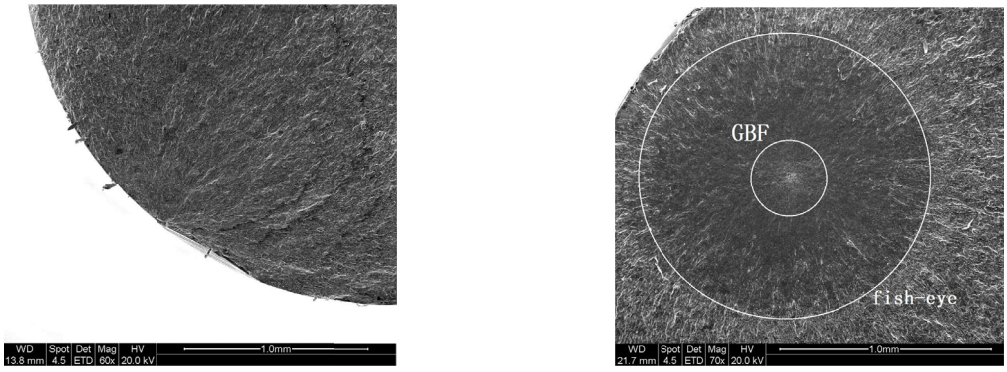

(a) The conventional observation (550 MPa, 4.21×10^6) (b) the ultrasonic observation (550 MPa, 2.07×10^7)

Fig. 4. Facture observations under different frequencies with the same stress amplitude

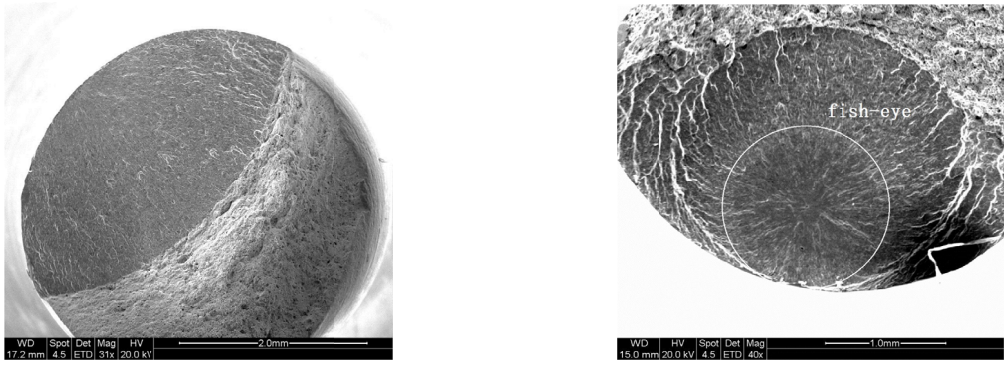

(a) The conventional observation (525 MPa, 7.12×10^6) (b) The ultrasonic observation (600 MPa, 7.44×10^6)

Fig. 5. Facture observation s under different frequencies with the same fatigue life

The observations indicate that the fracture mechanisms of these two are similar, but still some difference between these two. The "fish-eye" in the ultrasonic observation isn't captured clearly, it is because that the internal crack initiation location is far away from the surface and the variation of the propagation rate during the fatigue process is stable. The conventional observation shows a smooth flat surface and no GBF or "fish-eye" appeared in the fracture section which means that the fatigue failure occurred owing to surface roughness, but neither internal inclusions, nor the effect of hydrogen.

Another point can be seen clearly that, as shown in Fig. 3, the *S-N* curve obtained from the conventional experiment is obvious different from the ultrasonic one, it presents a trend of continuous decline but the ultrasonic *S-N* curve has three stages. However, some other significant differences can be found on the fatigue strength and fatigue life in two different loading frequencies of 140 Hz and 20 KHz.

2.4. The fatigue fracture surface observations

Some more examples of macroscopic fracture surface are presented in Fig. 5, where the results obtained at loading frequency of 140 Hz. It can be found that the fatigue crack initiates from the surface defects and the fatigue failure take place in the surface-induce fractures. But smooth specimen is employed in the fatigue experiments and no obvious defects can be detected in the specimen surface, so the occurred fatigue failures are caused by the surface roughness, which has been reported by Zhang [25]. Individual groove on the specimen surface caused by processing can be seen as a "fatigue crack" which can easily cause the stress concentration and result in the fatigue failure. In Fig. 6, it is clear that the fatigue failure occurs though the crack propagation of one single crack or multiple cracks. Fig. 6 (a) and Fig. 6 (b) indicate that only one crack is induced on the fracture surface, however that multiple cracks are obtained at the specimen surface in Fig. 6 (c) and Fig. 6 (d). The multiple cracks caused failure tends to have a shorter life than the one crack caused failure.

The failures at 140 Hz occurred in the mode of surface-induced fractures and no internal fatigue failures are detected. The radial fatigue striations at starting point of surface defect are clearly observed and the failure direction can be deduced according to the distributions of the fatigue striations as shown in Fig. 6 (a) to (d). This aspect due to the fact that the stress concentration around the groove can easily form the surface fatigue crack, thus the surface roughness is the primary factor leading to the surface fatigue failure.

Fig. 7 (a) to (d) are the observations obtained from the fracture surface at 20 KHz. All these observations have the same feature that the internal inclusion can be clearly detected and the corresponding fatigue life is at the VHCF level, more than that the failure direction appears as inclusion-centered radial striations.

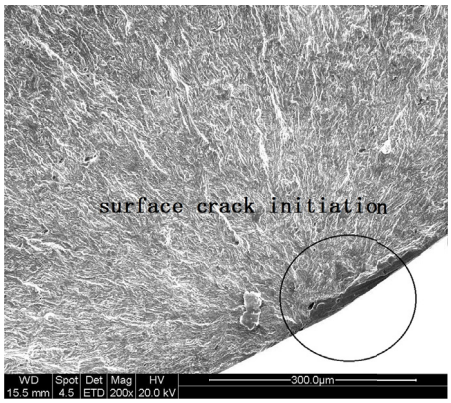

(a) Single crack initiation ($N_f = 1.76\times10^6$)

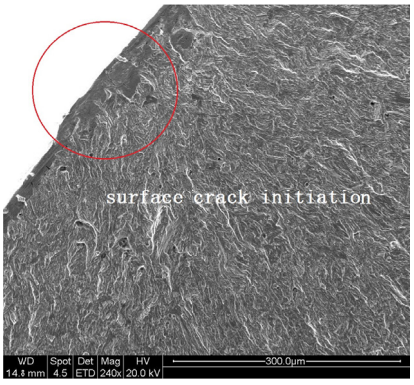

(b) Single crack initiation ($N_f = 7.12\times10^6$)

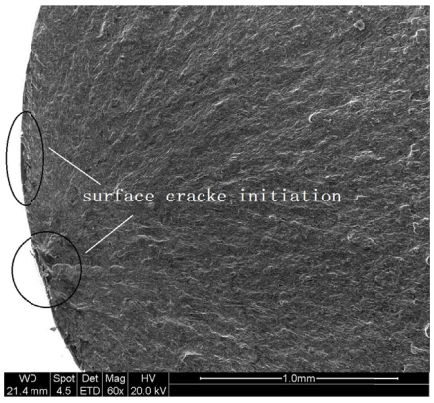

(c) Multiple crack initiations ($N_f = 7.50\times10^5$)

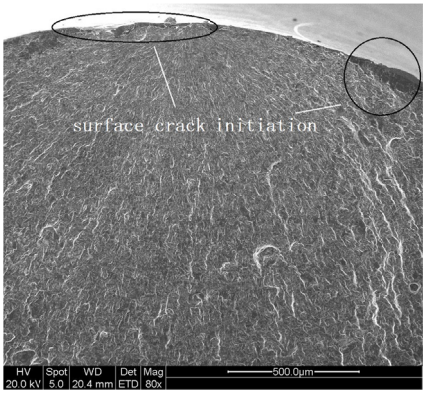

(d) Multiple crack initiations ($N_f = 1.41\times10^5$)

Fig. 6. The surface crack initiation at 140 Hz

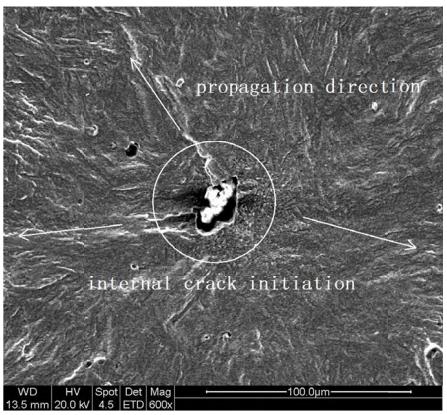

(a) Internal inclusion $N_f = 1.45\times10^7$

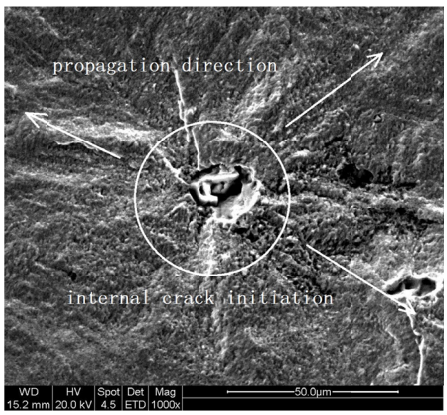

(b) Internal inclusion $N_f = 2.07\times10^7$

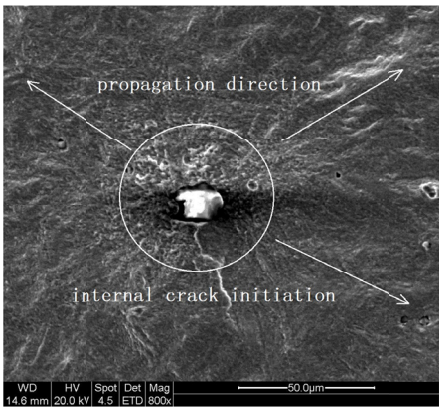

(c) Internal inclusion $N_f = 5.98\times10^7$

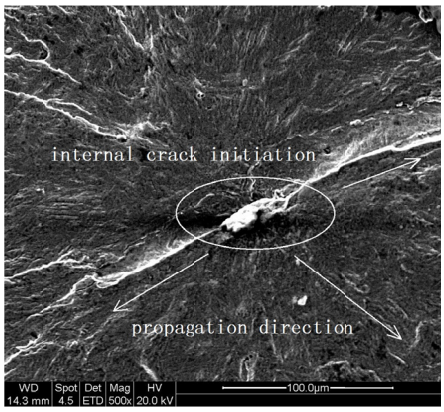

(d) Internal inclusion $N_f = 1.02\times10^7$

Fig. 7. The internal crack initiation at 20 KHz

It has been widely accepted that the very high cycle fatigue failure is due to subsurface crack propagation, and the internal inclusion sites are the common crack initiation locations. During the failure process, the hydride produced by the internal inclusion has a significant influence on the fatigue property of FV520B-I [25, 26]. GBF region (as shown in Fig. 4 (b)) is the most significant results caused by the hydrogen concentration. So the giga-cycle fatigue crack propagation can be divided into three stages: slow propagation of GBF; stable propagation from GBF to the boundary of "fish-eye"; and unstable propagation until the failure, just as shown in Fig. 4 (b) and Fig. 5 (b).

2.5. Discussions

Fig. 2 shows that the fatigue property of FV520B-I has some differences with the reported results of the loading frequency on the fatigue property. More than that, the observations show that the primary factors leading to the fatigue failure under 140 Hz and 20 KHz loading frequencies are different which imply that the FV520B-I fatigue properties under different loading frequencies are also different. In summary, this difference is caused by the influence of the obvious change of loading frequency [27-29], from 140 Hz to 20K Hz. The loading frequency used in the conventional experiment is almost 140 times lower than the ultrasonic experimental loading frequency, which means that the ultrasonic experimental stain is 2000-20000 times faster than the conventional one [30], this results in a significant difference in the stress distribution between these two experiments and the ultrasonic experiment will get a longer life than the conventional experimental one. So the ultrasonic experimental data can't be used directly to analysis the fatigue failure in the actual working condition, and it is necessary to establish the conversion model between two different loading frequencies to eliminate the effect of the frequency on the fatigue property of FV520B-I.

3. The FV520B-I fatigue property with loading frequency

Basquin formula has numerous advantages such as simple calculation process, reliable calculation results and extensive applicability [20-21]. It has been widely used to describe the relation between fatigue strength σ_a and fatigue life N_f [22,30], and the continuous decline stage of the *S-N* curve can be expressed by the Basquin formula effectively in both LCF and VHCF regime [31]. The formula can be expressed as:

$$\sigma_a = \sigma_f' \left(2N_f\right)^b \tag{1}$$

Where σ_α is fatigue strength (namely conditioned fatigue limit or the experimental stress amplitude); N_f is the fatigue life; $\sigma_f^{'}$ is fatigue strength coefficient; b is fatigue strength index. σ_f and b are constants for different loading frequencies and different materials. Different materials should have their own factors and no common values for FV520B-I can be used directly. So it is necessary to obtain the particular value for FV520BV-I to establish the conversion model for FV520B-I. Using the appropriate experimental data and Eq. (1), two empirical formulas for FV520B-I with different loading frequencies can be identified by model fitting and model parameters estimation.

3.1. The fatigue life conversion model for FV520B-I

According to Eq. (1) and the experimental data, the Basquin formulas for FV520B-I under 20 KHz and 140 Hz are written as:

$$\begin{cases} 20KHz:\ \sigma_{aH} = \sigma_{fH}^{'}\left(2N_{fH}\right)^{b_H} \\ 140Hz:\ \sigma_{aL} = \sigma_{fL}^{'}\left(2N_{fL}\right)^{b_L} \end{cases} \tag{2}$$

Where σ_{aH} and σ_{aL} are fatigue strength for 20 KHz and 140 Hz; N_{fH} and N_{fL} are fatigue life for 20 KHz and 140 Hz; $\sigma_{fH}^{'}$ is the fatigue strength coefficient for 20 KHz; b_H is the fatigue strength index for 20 KHz; $\sigma_{fL}^{'}$ is the fatigue strength coefficient for 140 Hz; b_L is the fatigue strength index for 140 Hz. These four parameters ($\sigma_{fH}^{'}$, b_H, $\sigma_{fL}^{'}$, b_L) are related to the material FV520B-I and they also have a strong relationship with the fatigue strength of metal. No common values can be used directly, so it is necessary to estimate the unknown parameters of FV520B-I based on the experimental data.

Fitting algorithm to data uses continuous curves or analytical expressions to represent discrete data and depict the functional relationship between the coordinates. The basic model has been established in Eq. (2). The iterative computation is used to determine the function $f(\sigma_a, N_{fi}^{'})$ by making the minimum value of $\sum_{i=1}^{n}\left(f\left(\sigma_a, N_{fi}^{'}\right)-N_i\right)^2$ as shown in Eq. (3) [32].

$$\begin{cases} \min\left(\sigma_{fH}^{'}, b_H\right) = \sum_{i=1}^{n}\left(f\left(\sigma_a, N_{fHi}^{'}\right)-N_{Hi}\right)^2 \\ \min\left(\sigma_{fL}^{'}, b_L\right) = \sum_{i=1}^{n}\left(f\left(\sigma_a, N_{fLi}^{'}\right)-N_{Li}\right)^2 \end{cases} \tag{3}$$

By using of the experiment data, the model parameters are estimated with the fitting algorithm [31], the results are shown in Table 3.

TABLE 3

The model parameters for FV520B-I

Frequency/factor	$\sigma_{fH}^{'}$	b_H	$\sigma_{fL}^{'}$	b_L
Estimation value	1365	–0.0532	1108	–0.0473

By substituting the parameters into the basic model (2), the empirical Basquin formulas for FV520B-I with 20 KHz and 140 Hz can be written as:

$$\begin{cases} 20KHz:\ \sigma_{aH} = 1365\left(2N_{fH}\right)^{-0.0532} \\ 140Hz:\ \sigma_{aL} = 1108\left(2N_{fL}\right)^{-0.0473} \end{cases} \tag{4}$$

At different loading frequencies, the relationship between the stress amplitude σ_α and fatigue life N_f are calculated according to Eq. (4), which is called the *S-N* curve. It is depicted as shown in Fig. 8.

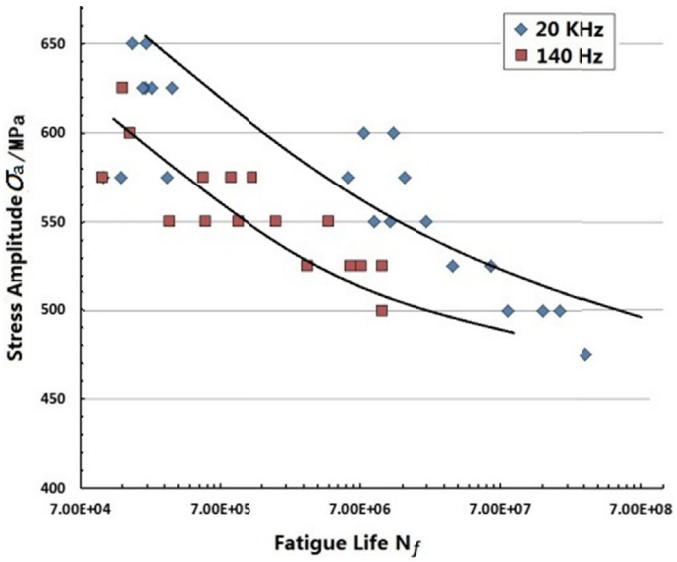

Fig. 8. The *S-N* curve depicted by Basquin formula

When the fatigue strength with different loading frequencies follow the relationship that $\sigma_{aH} = \sigma_{aL}$, according to Eq. (2), the relationship between the corresponding fatigue life (N_{fH} and N_{fL}) can be expressed as:

$$\left(2N_{fL}\right)^{b_L} = \frac{\sigma_{fH}^{'}}{\sigma_{fL}^{'}}\left(2N_{fH}\right)^{b_H} \tag{5}$$

Eq. (5) means that the ultrahigh loading frequency life N_{fH} can be converted to the conventional loading frequency life N_{fH}. And the quotient of fatigue strength coefficients ($\sigma_{fL}^{'}$ and $\sigma_{fH}^{'}$) is correction factor constant σ_0, it can be expressed as:

$$\sigma_0 = \frac{\sigma_{fL}^{'}}{\sigma_{fH}^{'}} \approx 0.812 \tag{6}$$

So the converted N_{fL} is calculated by substituting the ultrahigh loading frequency experimental data (N_{fH}) and model parameters (σ_0, b_H and b_L) into Eq. (5), the results are shown in Table 4.

Fig. 9 shows the distribution of the theoretical fatigue life calculated by Eq. (5) and the experimental data.

The errors between the results from the experimental data and the converted data are in a reasonable range and it proves the

TABLE 4

The fatigue life conversion

20 KHz N_{fH}	5.75e6	8.84e6	3.21e7	7.96e7	5.98e7	2.07e7
140 Hz (converted N_{fL})	5.35e5	8.68e5	3.70e6	1.03e7	7.44e6	1.76e6
140 Hz (experimental N_{fL})	5.22e5	9.35e5	2.96e6	1.00e7	7.12e6	2.26e6
Errors	2.49%	7.17%	25.00%	3.00%	4.49%	22.12%

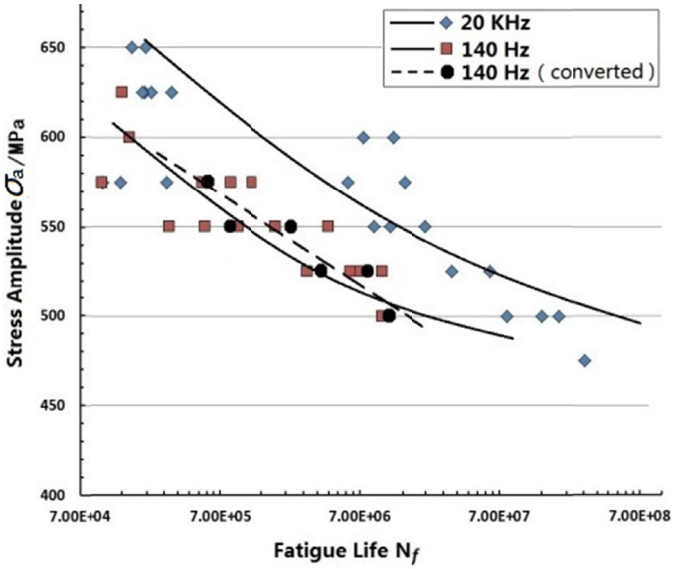

Fig. 9. The distributions of converted fatigue life and experimental data

accuracy of the experimental data. If the actual fatigue strength is known (or the actual fatigue strength can be estimated), the actual fatigue life can be calculated based on the experimental fatigue life under the same fatigue strength by Eq. (5). Thus, Eq. (5) is able to be used for the fatigue life conversion model for FV520B-I. It is proper also for the FV520B-I fatigue life translation, under the same fatigue strength, from the ultrahigh loading frequency experimental life to a conventional one. This model also can be used to eliminate the influence of ultrahigh loading frequency on the fatigue life for FV520B-I. An accurate fatigue strength estimation result is helpful to the fatigue life prediction, so *t* is necessary to establish a fatigue strength conversion model for FV520B-I to eliminate the influence of the ultrahigh loading frequency on the fatigue strength estimation.

3.2. The fatigue strength conversion model for FV520B-I

According to Eq. (2), the fatigue strength correction factor σ_{ac} is the quotient of σ_{aL} and σ_{aH}, it can be expressed as:

$$\sigma_{ac} = \frac{\sigma_{aL}}{\sigma_{aH}} \tag{7}$$

Difference value of the fatigue strength index Δb can be written as:

$$\Delta b = b_L - b_H \tag{8}$$

Four parameters σ'_{fH}, b_H, σ'_{fL} and b_L are all constant as shown in Table 2, so $\sigma_0 = 0.812$ and $\Delta b = 0.0059$. Then, substituting Eq. (6) and Eq. (7) into Eq. (2), thus it can be re-expressed as:

$$\sigma_{ac} = \sigma_0 \frac{\left(2N_{fL}\right)^{b_L}}{\left(2N_{fH}\right)^{b_H}} \tag{9}$$

If the fatigue life data obtained from ultrasonic experiment (N_{fH}) and conventional experiment (N_{fL}) are equal or similar, $N_{fH} \approx N_{fL}$, so Eq. (9) will be transformed as:

$$\sigma_{ac} = \sigma_0 \frac{\left(2N_{fL}\right)^{b_L}}{\left(2N_{fH}\right)^{b_H}} \approx \sigma_0 \left(2N_{fL}\right)^{b_L - b_H} = \sigma_0 \left(2N_{fL}\right)^{\Delta b} \tag{10}$$

The difference value of fatigue strength index Δb (Δb = 0.0059) is a constant close to 0 which means that $(2\ N_{fL})^{\Delta b} \approx 1$, so the he relationship between fatigue strength correction factor σ_{ac} and correction factor constant σ_0 should be:

$$\sigma_{ac} \approx \sigma_0 \tag{11}$$

So, by substituting the experimental data (N_{fL} and N_{fH}) into the Eq. (10), the fatigue strength correction factor σ_{ac} could be calculated and the results are shown in Table 5.

TABLE 5

Fatigue strength correction coefficient

20 KHz	N_{fH}	5.75e6	7.44e6	8.84e6	1.14e7
140 Hz	N_{fL}	5.97e6	7.16e6	1.00e7	1.00e7
	σ_{ac}	0.892	0.890	0.890	0.901
	σ_0	0.812			

But the estimation data in Tab.4 indicate that the two factors ($\sigma_{ac} \approx 0.893$ and $\sigma_0 = 0.812$) don't follow the relation in Eq. (11).

If fatigue strength correction factor σ_{ac} and correction factor constant σ_0 follow the Eq. (11), $\sigma_{ac} \approx \sigma_0 = 0.812$, so the conversion relationship between σ_{aL} and σ_{aH} can be expresssed as:

$$\sigma_{aL} = \sigma_{ac} \cdot \sigma_{aH} = \sigma_0 \cdot \sigma_{aH} \tag{12}$$

According to Eq. (12), converted fatigue strength (from 20 KHz to 140 Hz), experimental data (140 Hz) and the errors are shown in Table 6.

The minimum error is 7.4% and the maximum one is 15.8% and the average of errors is 11%. At this time, a new material frequency correction factor f_σ for FV520B-I must be introduced in Eq. (11) to modify the relationship between σ_{ac} and σ_0.

f_σ is proposed to add because of effect of the loading frequency on the fatigue failure that results in the difference between the fatigue mechanism of very high cycle-fatigue failure and the

TABLE 6

Converted fatigue strength and errors based on Eq. (12)

Converted strength (20KHz)/MPa	465	505	486	505	463	445	506
Experimental data (140Hz)/ MPa	525	550	525	600	525	500	575
Errors	11.4%	8.2%	7.4%	15.8%	11.8%	11.0%	12.0%

conventional fatigue as discussed in chapter 2. Another reason is that the distribution of the experimental data shows a significant discreteness. This is because of FV520B-I's specific fatigue property [24], which is very sensitive to loading frequency and stress amplitude – small change of stress amplitude in experiment will result in a huge fluctuation on fatigue life prediction. These influences will be echoed and controlled by the new factor f_σ. This factor is necessary and can't be neglected in the process of fatigue strength conversion. And different metals should have their own specific factor constants.

Here the material frequency correction factor $f_\sigma = 1.099$, so the relationship between σ_{ac} and σ_0 is improved as:

$$\sigma_{ac} \approx f_\sigma \sigma_0 = 1.1 \times 0.812 \approx 0.893 \tag{13}$$

So σ_{aH} can be converted to σ_{aL}, and they follow the relationship as:

$$\sigma_{aL} = \sigma_{ac} \cdot \sigma_{aH} = \sigma_0 \cdot f_\sigma \cdot \sigma_{aH} = 0.893 \times \sigma_{aH} \tag{14}$$

Table 7 shows the converted fatigue strength (from 20 KHz to 140 Hz), experimental data (140 Hz) and the errors.

The distributions of the converted fatigue strength and the experimental data are shown in Fig. 10.

As shown in Table 6 and Fig. 10, the maximum is 7.3%, the minimum is 1.1% and the average is about 3%, the errors obtained by Eq. (14) are much smaller than the errors shown in Table 5. The errors between the converted fatigue strength and conventional strength are all within an acceptable tolerance. The ultrasonic fatigue strength revised by f_σ is more close to the conventional one, so the proposition of the new frequency correction factor f_σ is acceptable.

More than that, the converted fatigue strength is almost consistent with the experimental data (140 Hz) and they also have the same distribution trend. Most of the converted results are smaller than the experimental value, which means that the converted results are conservative and safer in use for the actual working condition. Thus the proposed Eq. (14) can be used to convert the fatigue strength under different loading frequencies.

On errors of model, they may result from these resources:

1. System errors (both Fatigue Test System and data acquisition system errors) will affect the life prediction process. If the experiment is carried out without precision calibration beforehand, little deviation of the measurement of the displacement could cause a big error in the fatigue life result.
2. Although the specimen used in the experiment were from the same batch production, there yet some differences among them, especially in the micro-morphology level. Since these differences are difficult to tell and often neglected in the experiment and following analysis process, the results will contain mistreated errors.
3. The calculation results are not comprehensive as the existence of some undetected defects may also lead to errors. Interference factors such as humidity and dust during the experiment will affect the precision and result with errors.
4. FV520B-I may have a special fatigue property, which may be very sensitive to the surface roughness and stress amplitude – small change of stress amplitude in experiment will result in a huge fluctuation on the experimental results. But the "sensitivity" is just a hypothesis and more effort is needed for looking into it.

This type of combination of errors leads to the resultant error between the converted result and experimental result. As discussed above although the errors exist, they are within an acceptable tolerance and model predicted value is smaller than

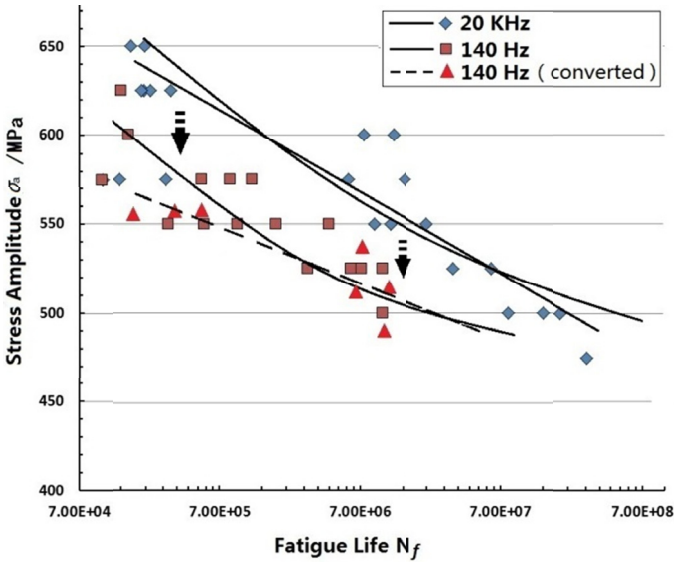

Fig. 10. The distributions of converted fatigue strength and experimental data

TABLE 7

Converted fatigue strength and errors based on Eq. (14)

Converted strength (20 KHz)/MPa	512	556	535	556	510	490	557
Experimental data(140 Hz)/MPa	525	550	525	600	525	500	575
Errors	2.5%	1.1%	1.9%	7.3%	2.9%	2.0%	3.1%

that in experiment result, which results in a conservative estimation and safer situations in practice. The fatigue life and strength models can be adapted to providing a meaningful prognostic for preventive maintenance, and be used for fatigue analysis of FV520B-I to avoid sudden catastrophic failure of mechanical systems in real applications.

4. Conclusions

First, FV520B-I appears to be a different property compared to the other metal materials, and the fatigue limit of FV520B-I tends to decrease with the increase of the loading frequency. The increase of loading frequency is beneficial for the improvement of fatigue life. High loading frequency could result in long fatigue life, but low fatigue limit. And FV520B-I appears to be a sensible choice for the change in the stress amplitude. A small change of the stress amplitude will result in a significant change of fatigue life.

Second, surface roughness is the primary factor leading to the fatigue failure of FV520B-I at 140 Hz. The fatigue failure takes place in the model of surface-induced fracture, and the internal inclusion is the main reason of fatigue failure of FV520B-I at 20 KHz. This difference is due to the changing of loading frequency.

Third, a *new* material frequency correction factor f_σ ($f_\sigma = 1.1$) related to FV520B-I is proposed and introduced in the fatigue strength conversion model. The material frequency correction factor (f_σ) made it possible to convert the ultrahigh loading frequency fatigue strength into the conventional one with a high approximate-ness.

Fourth, four model parameters (σ'_{fH}, b_H, σ'_{fL}, b_L) for FV520B-I are obtained from experimental data fitting.

Fifth, the FV520B-I fatigue life conversion model (Eq. (5)) and the fatigue strength conversion model (Eq. (14)) are proposed.

The determination of f_σ and the establishment of the conversion models improve the accuracy of fatigue analysis results in engineering practice, and also make it possible to process the pertinent fatigue life prediction and remanufacturing processes involving FV520B-I. This study about the effect of ultrahigh loading frequency on the fatigue strength of FV520B-I makes up the deficiency of FV520B-I fatigue data, and also enriches the fatigue property data of FV520B-I.

This study is a frame work of a potential research study worth further investigation and deeper understanding: 1) More experiments are required to prove the proposition about the sensibility of FV520B-I to stress amplitude; 2) more fatigue experiments with various loading frequencies and insight work on special fatigue properties are needed to prove the applicability and feasibility of the factor f_σ and σ_{ac} for FV520B-I; 3) the fatigue strength formula should be modified by adding more factor parameters, estimated by more designed experiments, which will result in a fine fatigue strength model with high accuracy of model prediction and conversion.

This research on the influence of ultrahigh loading frequency to the fatigue property of FV520B-I still faces numerical challenges in theory and applied modeling technology. These concerns discussed in this paper are open to future research investigation and study.

Acknowledgement

The authors gratefully acknowledge the research funding support from the National Key Base Research and Development Program of China (No. 2011CB013401) and The National Natural Science Foundation of China (No. 51375074 & No. 51475077). Also thanks are due to Professor Sun Qingchao, Shi Bowen for their technical support.

REFERENCES

[1] M. Zhang, W.Q. Wang, P.F. Wang, Y.N. Liu, J.F. Li. Pro. Mate. Scie. **3**, 2035-2041 (2014).
[2] K. Wang, F. Wang, W. Cui, T. Hayat, B. Ahmad, Fatigue. Fract. Eng. M. **37** (10), 1075-1086 (2014).
[3] T. Machniewicz, Fatigue. Fract. Eng. M. **36**, (4), 361-373 (2013).
[4] C.M. Suh, M.S. Suh, S.G. Kim, Fatigue. Fract. Eng. M. **35** (1), 30-36 (2012).
[5] K.L. Fan, X.S. Liu, G.Q. He, H. Cheng, Z. Zhang, Mater. Charact. **107**, 239-248 (2015).
[6] A. Kumar, N. Singh, V. Singh, Mater. Charact. **51** (4), 225-233 (2003).
[7] J.M. Herrera, P.R. Spencer, P. Tarin, S.W. Stafford, Mater. Charact. **33** (1), 33-35(1994).
[8] Y. Yang, Y.B. Liu, Mater. Charact. **59** (5), 567-570 (2008).
[9] D.H. Jeong, M.J. Choi, M. Goto, H.C. Lee, S. Kim, Mater. Charact. **95**, 232-244 (2014).
[10] X.Y. Jiang, Study on Ultrasonic fatigue of 40CrNiMoA Steel, PhD thesis, Jiang Su University, Zhenjiang, 2008.
[11] H.Q. Xue, Investigation on Fatigue Behavior of Materials in Very High Cycle Regime under Vibratory Loading, PhD thesis, Northwestern Polytechnical University, Xi'an, 2006. (in Chinese)
[12] H.F. Yi, Effect of ultrasonic frequency on giga-cycle fatigue properties of steel, PhD thesis, Southwest Jiaotong University, Chengdu, 2011.
[13] M.L. Zhu, L.L. Liu, F.Z. Xuan, Int. J. Fatigue. **77**, 166-173 (2015).
[14] B. Guennec, A. Ueno, T. Sakai, M. Takanashi, Y. Itabashi, Int. J. Fatigue. **66**, 29-38 (2014).
[15] J. Dahal, K. Maciejewski, H. Ghonem, Int. J. Fatigue. **57**, 93-102 (2013).
[16] H. Wang, Study of fatigue behavior and mechanism of fatigue failure in the ultra-high-cycle regime in 40Cr and 50 axles steels, PhD thesis, Southwest jiaotong university, Chengdu 1998.
[17] Y.M. Wang, J.N. Univ. **15** (3), 41-45(1994).
[18] S.S. Yan, J.C. Jien, Nucl. Eng. Des. **191**, 225-230 (1999).
[19] S. Stanzl, R. Mitsehe, Advances in Research on the Strength & Fracture of Materials, 1978 Waterloo.

[20] S. Schmid, M. Hahn, S. Issler, H.M. Bacher, Int. J. Fatigue. **60**, 90-100 (2014).
[21] A. Zhao, J. Xie, C. Sun, Z. Lei, Y. Hong, Int. J. Fatigue. **38**, 46-56 (2012).
[22] M L. Zhu, L.L. Liu, F.Z. Xuan, Int. J. Fatigue. **77**, 166-173 (2015).
[23] G. Benjamin, U. Akira, S. Tatsuo, T. Masahiro, I. Yu. Int. J. Fatigue. **66** (6), 29-38 (2014).
[24] J.L. Wang, Y.L. Zhang, Q.C. Sun, S.J. Liu, B.W. Shi, H.T. Lu, Mater. Design. **89**, 1024-1038 (2016).
[25] M. Zhang, W.Q. Wang, P.F. Wang, Y. Liu, J.F. Li, Int. J. Fatigue. **87**, 22-37 (2016).
[26] J. Wang, Y. Zhang, S. Liu, Q. Sun, H. Lu, Int. J. Fatigue. **87**, 203-209 (2016).
[27] T.S. Stanzl, Int. J. Fatigue. **60**, 2-17 (2014).
[28] J.W. Zhang, Q.P. Song, N. Zhang, L.T. Lu, M.T. Zang, G.D. Cui, Int. J. Fatigue. **70**, 235-240 (2014).
[29] H. Mayer, R. Schuller, M. Fitzka, Int. J. Fatigue. **57**, 113-119 (2013).
[30] P. Gillis, Effect of Strain Rate on Flow Properties Metals Handbook. Ninth Edition, USA Ohio, ASM **8**, 38-46 (1985).
[31] H. Wang, Study of fatigue behavior and mechanism of fatigue failure in the ultra-high-cycle regime in 40Cr and 50 axles steels, Ph.D thesis, Southwest jiaotong university, 1998.
[32] Y.L. Zhang, J.L. Wang, Q.C. Sun, H. Zhang, P.S. Jiang, Mater. Design. **69**, 241-246(2015).